Cellulose (2021) 28:10457–10475
https://doi.org/10.1007/s10570-021-04195-w

ORIGINAL RESEARCH

High oxygen barrier chitosan films neutralized by alkaline nanoparticles

Urška Jančič · Mojca Božič · Silvo Hribernik · Tamilselvan Mohan · Rupert Kargl · Karin Stana Kleinschek · Selestina Gorgieva

Received: 24 May 2021 / Accepted: 13 September 2021 / Published online: 21 September 2021

Abstract The most frequent neutralisation procedure, applied on chitosan (CS) films includes treatment with NaOH base. Such treatment endows CS films with stability in water, yet, same can significantly decrease the film performance. In the present paper, we investigate $Mg(OH)_2$ nanoparticles as a neutralisation agent for CS solutions followed by casting into films. This is combined and compared with classical casting and film drying from non-neutralized solutions followed by NaOH treatment after film formation. The influence on the properties of resulting films is investigated in detail and large differences are found for structure and barrier properties. The stable, opaque-to-transparent CS films (depending on $Mg(OH)_2$ content and post-treatment) were obtained by facile casting method of neat CS or CS–$Mg(OH)_2$ dispersions, in the complete absence of cross-linkers and plasticizers. FTIR data demonstrate the $Mg(OH)_2$ and NaOH deprotonation effect, and strongly suggest intensive H-bonding interaction between CS and $Mg(OH)_2$. X-ray photoelectron spectroscopy showed differences in the hydroxide content and protonation of CS nitrogen. The reduction of surface roughness and increase of homogeneity, the tensile strength and elongation, as well as thermal stability and excellent oxygen barrier properties were measured for CS enclosing the $Mg(OH)_2$ nanoparticles. Further treatment with 1 M NaOH causes repacking of CS polymer chains, improving the crystallinity and water vapour barrier properties, degrading the mechanical properties by increasing the films brittleness and increasing the char formation due to reduced thermal stability.

U. Jančič · S. Hribernik · T. Mohan · S. Gorgieva (✉)
Faculty of Mechanical Engineering, Institute of Engineering Materials and Design, University of Maribor, Smetanova ulica 17, 2000 Maribor, Slovenia
e-mail: selestina.gorgieva@um.si

M. Božič
Dravske Elektrarne Maribor d. o. o., Obrežna Ulica 170, 2000 Maribor, Slovenia

S. Hribernik · R. Kargl · K. S. Kleinschek · S. Gorgieva
Faculty of Electrical Engineering and Computer Science, Institute of Automation, University of Maribor, Koroška cesta 46, 2000 Maribor, Slovenia

T. Mohan · R. Kargl · K. S. Kleinschek
Institute of Chemistry and Technology of Biobased Systems (IBioSys), Graz University of Technology, Stremayrgasse 9, 8010 Graz, Austria

Graphic abstract

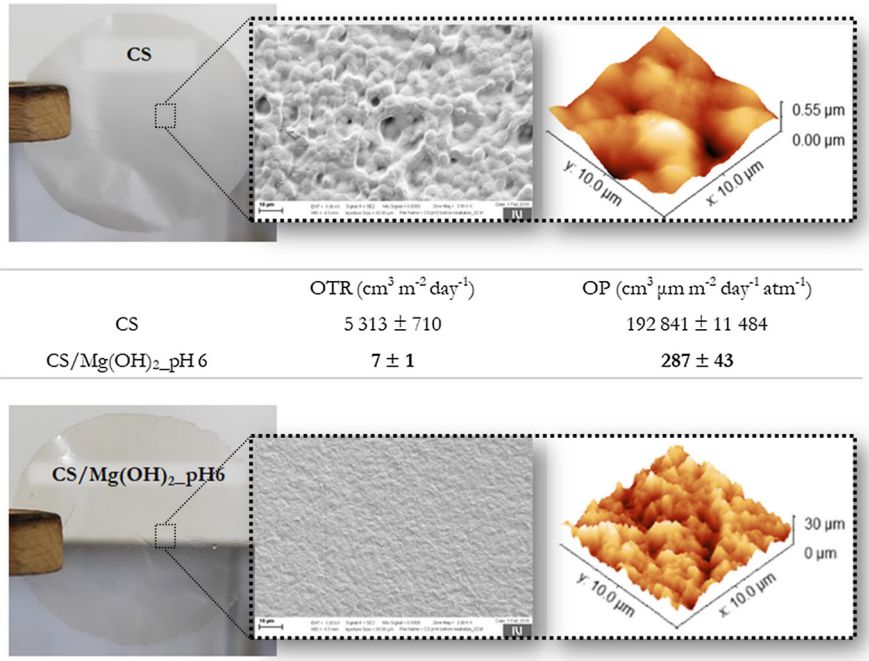

Keywords CS films · $Mg(OH)_2$ · Neutralization · Microstructure · Oxygen barrier properties

Introduction

Chitosan (CS) is a pseudo-natural, deacetylated chitin product, originated from exoskeletons of arthropods (including crustaceans and insects), marine diatoms and algae, as well as some fungal cell walls. CS is one of the few native polysaccharides with primary amines leading to a positively charged polyelectrolyte under acidic conditions, triggering its solubility, and ultimate properties as well. Due to a multitude of interesting features (e.g. nontoxicity, biodegradability, hydrophilicity, antimicrobial and antifungal efficiency, film-forming capacity) offered by CS macromolecules comprising randomly distributed fractions of β-(1 → 4)-D-glucosamine and β-(1 → 4)-N-acetyl-D-glucosamine, this polymer evidence promise in various fields. Some of them are food packaging (Božič et al. 2011, 2012; Manigandan et al. 2018), cosmetics (Hirano et al. 1991), biomedicine (Gorgieva and Kokol 2012; Reddy Tiyyagura et al. 2016; Gorgieva et al. 2018; Wang et al. 2020), agriculture (Bandara et al. 2020), wastewater management (No and Meyers 2000), fuel cells (Kaker et al. 2019; Gorgieva et al. 2021; Hren et al. 2021), etc. CS films have been successfully used as packaging materials to preserve the quality of a wide variety of fruits (raspberry, apple, kiwi (Drevinskas et al. 2017), strawberry) and even meats (chicken, turkey, beef, pork, and fish) (Homez-Jara et al. 2018). Besides, the CS is also known to elicit plant defences against several classes of pathogens, including fungi, viruses, bacteria and phytoplasma, widening its use also in pharmacy (Shariatinia 2019). CS possesses the excellent capacity to form microspheres, membranes and fibres, mainly using acetic acid as solvent, or other alternative solvents, such as lactic (Niamsa and Baimark 2009), tartaric (Cui et al. 2018), maleic, hydrochloric and nitric acid, adipic, and citric acid (Hejazi et al. 2018) as well as inorganic $AlCl_3{\cdot}6H_2O$(Hu et al. 2018) all of which influence final mechanical properties. The solubility in such, semi-aquatic environments and diluted acidic solutions, contributes to high moisture absorption, diminishing

the mechanical properties as well, for which different plasticizers, fillers, or cross-linking agents have been used (Hejazi et al. 2018; Gorgieva et al. 2018).

The film formation out of CS solution occurs due to the preservation of chain entanglements and intermolecular interactions (e.g. H-bonding) during the drying process. The neutralization of CS films, membranes, or nano/microparticles that are prepared by drying acidic solutions followed by immersion into NaOH is the most frequently used neutralisation approach to omit their solubility while eliciting other properties for the resulting material. Indeed, the neutralization was found to significantly influence the proliferation and cytoskeletal organization of chondrocytes seed it on CS-based matrices (Noriega and Subramanian 2011). Effects of neutralization on the physicochemical properties on antibacterial, and drug-release properties also have been reported (Mauricio-Sánchez et al. 2018). Yet, as a strong base, the NaOH can be rather aggressive towards biopolymers. It was already demonstrated that CS films treated with aqueous, 0.1–1 M NaOH revealed not only deprotonation responsible for solubility reduction, but also increase the deacetylation, influencing the packaging and ordering of molecules and crystallinity of resultant films (Takara et al. 2015). This post-processing procedure can even devalue the CS films applicability in a segment where CS acetyl groups can contribute, for instance, in the stabilization of crystalline structures which plays an important role in mechanical behaviour (Cui et al. 2016), as well as in hydrophobicity. We, therefore, became interested in how the pH value of the CS solution that is used to cast films, influences the structure and properties of resulting films after drying. An alternative to neutralization after casting and drying is partial neutralization of the CS solution before processing into films. Acidic aqueous CS solutions can however not easily and quickly be neutralized by the addition of liquid bases because local gelling occurs.

Therefore, we examine the effects of inorganic $Mg(OH)_2$ nanoparticles a neutralisation agent for CS films added before film casting. $Mg(OH)_2$ has been chosen because in pre-experiment it turned out that aqueous NaOH of sufficient concentration cannot be added quickly enough to the casting solutions without causing local gelling and an inhomogeneous polymer phase. $Mg(OH)_2$ is a weak base with very limited solubility in water (the Ksp at 25 °C is 6×10^{-12}). Indeed, the $Mg(OH)_2$ is widely used as an antacid since it slowly dissolves as it neutralizes stomach acid rather than dissolving all at once. During this reaction, the H^+ ions from the HCl in the stomach react with the OH^- ions from $Mg(OH)_2$ dissolution, forming water and driving the reaction to the right, causing more $Mg(OH)_2$ to dissolve and further dissociate. According to LeChâtelier's principle, the OH^- ions are removed from the solution by the H^+ ions, and more $Mg(OH)_2$ is forced to dissociate to replace those ions. These nanoparticles are non-toxic, low-cost material, which is often used as an additive in drugs and food sectors, offering among others the antibacterial, antifouling properties, flame retardant properties, etc. The addition of $Mg(OH)_2$ was already reported to support the formation of stable membranes for fuel cell application (Kaker et al. 2019; Hren et al. 2021) and to improve the compressive strength of CS/silk fibroin films for biomedical application (Eivazzadeh-Keihan et al. 2021), without details about the chemistry behind, and not in light of potential packaging application.

We assume that acidity of CS solution (dissolved in HCl) will trigger the step-wise solubility of $Mg(OH)_2$ nanoparticles, ending up with prolonged CS deprotonation in contrast to swift deprotonation with a strong base (as NaOH). Ultimately, we aim to demonstrate a relatively simple method for CS films processing, while investigating the $Mg(OH)_2$ neutralisation effect on few applicable properties of resulting films, when used alone, or combined with 1 M NaOH treatment. We hypothesise that a higher pH value of the film-forming solution leads to tighter packing of the polymer chains and henceforth higher barrier properties against oxygen or water vapour of resulting films.

Experimental

Materials

Chitosan (CS) (degree of deacetylation 90%, molecular weight: 50–100 kDa) was purchased in powder form with particle sizes below 200 µm from Biolog Heppe GmbH, Germany. Magnesium hydroxide ($Mg(OH)_2$) nanoparticles with size < 100 nm, sodium hydroxide (NaOH) and hydrochloric acid (HCl) were purchased from Sigma-Aldrich, Germany. All chemicals were used as received.

Film preparation

CS polymer was dissolved in Milli-Q water at 1.5 wt.% concentration, by adjusting the pH to 2.0 (with 1 M HCl) at room temperature. The resulting solution was stirred for 3 h until the solution mixture became homogeneous with a viscous, transparent appearance. To this solution, the 1 wt.% $Mg(OH)_2$ water dispersion was added to reach pH 4.0 or pH 6.0. The solution was diluted to the final 1 wt.% of CS and 6.9 mM of $Mg(OH)_2$ and 12.6 mM of $Mg(OH)_2$ at pH 4.0 and pH 6.0, respectively. 25 ml CS/$Mg(OH)_2$ dispersion were separately cast into a Petri dish with a diameter of 8.5 cm and allowed to dry at room temperature. For comparison 25 ml CS solution pH 2.0 was cast without adding $Mg(OH)_2$. Resulting, dry films were neutralized in 1 M NaOH for 30 min under slight shaking at room temperature, washed with Milli-Q water until pH of the washing Milli-Q water was constant and left to dry in the air (samples are indicated as n for neutralization with NaOH after casting). Comparisons were made with non-NaOH neutralized films. The as-prepared films were equilibrated at 50 ± 2% relative humidity (RH) and 21 ± 2 °C for 1 week and sealed in plastic bags until testing.

Morphology – FE-SEM and AFM

Field Emission Scanning Electron Microscopy (FE-SEM) measurements were performed with a Carl Zeiss FE-SEM SUPRA 35 VP electron microscope. For all samples, imaging was performed in a high vacuum at 1 kV accelerating voltage. The films were placed on a conductive carbon adhesive tape, mounted on an aluminium sample holder, air-dried and sputtered with Pd on chemical vapor deposition (CVD) sputtering device Denton (Denton Vacuum).

Atomic Force Microscopy (AFM) was performed in tapping mode with an Agilent 7500 AFM multimode scanning probe microscope (Keysight Technologies, Santa Barbara, USA). The images were scanned in tapping mode with silicon cantilevers (ATEC-NC, Nanosensors, Germany) at an ambient temperature in air (resonance frequency of 210–490 kHz and a force constant of 12–110 N m^{-1}). All images were recorded with a resolution of 2048 × 2048 pixels and were processed using the freeware Gwyddion allowing for the AFM roughness to be calculated as the root mean square (RMS) deviation from the mean height of the topography after levelling off the images by mean plane subtraction (Nečas and Klapetek 2012).

Contact angle measurements

The water contact angles of the films were measured by using Dataphysics contact angle measurement system OCA35 (Filderstadt, Germany) with the sessile drop (3 µl drop volume) method using the tangent method. Water absorption kinetics was monitored in time intervals until complete absorption. All measurements were performed at room temperature, in triplicates, and mean/standard deviation values were calculated.

Attenuated total reflectance fourier transform infrared spectroscopy (ATR-FTIR)

ATR-FTIR spectra were recorded using a Perkin-Elmer Spectrum One FTIR spectrometer with a Golden Gate ATR attachment and a diamond crystal at room temperature i.e., 23 ± 2 °C. The absorbance measurements were carried out within the 400–4000 cm^{-1}, with 16 scans and a resolution of 4 cm^{-1}.

X-ray diffraction (XRD)

XRD patterns of the membranes were collected on a D5005 X-ray diffractometer (Bruker Siemens). A diffraction angle 2 θ between 2° and 70° with a step size of 0.04° using Cu-kα radiation at 40 kV and 40 mA was measured. The background runs were subtracted from data runs, as suggested by French (2020) as an important step in XRD data treatment. The crystallinity (%) was calculated by dividing the area of the crystalline peaks by the total area under the curve from 2θ 5° to 30° (Abdou et al. 2008), using the Diffrac.eva software (Bruker).

X-ray photoelectron spectroscopy (XPS)

XPS analyses were carried out on the PHI-TFA XPS spectrometer produced by Physical Electronics Inc. The analyzed area was 0.4 mm in diameter and the analyzed depth was about 3–6 nm. The sample surfaces were excited by X-ray radiation from a

monochromatic Al source at a photon energy of 1486.6 eV. The high-energy resolution spectra were acquired using an energy analyzer operating at a resolution of about 0.65 eV and pass-energy of 187 eV. During data processing the spectra from the surface were aligned by setting the C–C/C–H peak in the C 1 s spectrum to binding energy of 285.0 eV. The accuracy of the binding energy was about ± 0.3 eV. The concentrations were calculated from the intensities of the peaks within the XPS spectra using relative sensitivity factors provided by the instrument's manufacturer. Two spots were analyzed on each sample and the average composition was calculated.

Binding energies (BE) were referred to as the C 1 s line of adventitious carbon at 284.8 eV and determined with the resolution of ± 0.1 eV. These spectra were fitted assuming Gaussian distribution for each peak, with a linear background to determine the binding energy of the various element core levels.

Oxygen permeability (OP)

The thickness of the films was measured by using a digital micrometre (Tesa, Swiss). Thicknesses of films were measured at several positions on the film and average values were calculated and used for following OP and Water vapour permeability (WVP) measurements.

Before measuring the oxygen transmission rate (OTR), the samples were conditioned at a temperature of 21 ± 2 °C and 50 ± 5% RH for 24 h. OTR of the films was determined according to ASTM D 3985–06 standard at 23 ± 2 °C and 50 ± 5% RH using an Oxygen Transmission Rate Test System (OX2/230, Labthink). The OTR was measured after the film had been placed in a cell and the oxygen flow introduced on one side of the film. The OP (cm^3 μm m^{-2} day^{-1} - $atm^{-}1$) was calculated from the mean OTR (cm^3 m^{-2} day^{-1}) multiplied by the film thickness (μm) and divided by the oxygen gradient within the cell of the testing machine. Three independent determinations were carried out for each film sample and mean/SD values were calculated.

Water vapour permeability (WVP)

Films were conditioned for 24 h were fixed above aluminium cups, each containing 45 g of calcium chloride. The whole device was weighed and then placed within a climatically controlled chamber (21 ± 2 °C and 50 ± 2% RH). The cups were then weighed at regular time intervals, and a linear relationship was obtained between the quantity of water transferred per unit of air and time. Water vapour permeability (g·m/m^2·h·Pa) was calculated as follows:

$$\mathrm{WVP} = (\mathrm{WVTR} \cdot l)/\Delta \mathrm{p} \quad (1)$$

where WVTR was measured water vapour transmission rate (g/m2·h) through a film specimen, l was average film thickness (m), and Δp was partial water vapour pressure difference (Pa) between the 2 sides of the film specimen. WVTR was determined gravimetrically using an ASTM Method E 96–95 (ASTM 1995). Three independent determinations were carried out for each film sample, and the mean/SD values were calculated.

Moisture content (MC)

The moisture content of films was determined by measuring the weight loss of films, upon drying in a halogen moisture analyzer (HB43 Mettler Toledo) at 105 °C. Before measurements samples were conditioned at a temperature of 21 ± 2 °C and 64% ± 2% RH for 24 h.

Thermal analysis

Differential scanning calorimetry (DSC) was performed using a thermal analyzer (TGA/DSC STAR System, HP DSC Mettler Toledo). Piece of films, weighing ~ 10 mg, were placed into aluminium pans and hermetically sealed. An empty pan was used as a reference. The samples were heated from 25 to 600 C at a constant rate of 10 °C/min, under a nitrogen atmosphere.

Thermogravimetric analysis (TGA) was performed using a thermogravimetric analyzer (TGA/DSC STAR System, HP DSC Mettler Toledo). The percentage weight loss and thermal degradation temperature values of the CS films were determined over the temperature range of 25–600 °C, using a heating rate of 10 °C/min, under a nitrogen stream.

Mechanical properties

The tensile strength at maximum (MPa) and the tensile strain at break (%) of the films were measured according to the standard method TAPPI T494 om-01 using a Shimadzu AGS-X electromechanical universal testing machine. For testing, the films were cut into a size of 4 mm × 5 cm and vertically mounted with two clamps with a 2.5 cm distance between the clamps. Films were tested at a speed of 1 mm min^{-1} with a 5 kN load cell. At least five experimental runs were carried out and average values and standard deviations were calculated. All films were conditioned at 21 ± 2 °C and 50 ± 2% RH for 24 h before the test.

Results and discussion

Morphology

Neat CS films were prepared out of 1% CS solution with pH 2, using 1 M HCl as solvent. The addition of different amounts of $Mg(OH)_2$ to CS solution, causes partial dissolution of the basic nanoparticles and release of hydroxyl ions, which increase the alkalinity of the system to pH 4 and 6 when 6.9 mM and 12.6 mM of $Mg(OH)_2$ are used. This avoids immediate local precipitation and gelling as would be the case when a solution of NaOH is added to and mixed with the CS solution. It rather leads to slower neutralization by the dissolution of the dispersed particles in the acidic solution. This should in turn cause the formation of a homogeneous CS solution with a higher pH value for casting and film formation. Films were cast, dried, neutralized with 1 M NaOH, washed with water and re-dried before analysis.

Macroscopic observation of neat cast acidic CS film (photographs on Fig. 1, left column) reveals opacity, which does not significantly alter after neutralization with 1 M NaOH (nCS film). On contrary, the addition of $Mg(OH)_2$ into CS solution, ends up in semi-transparent films, where higher transparency was observed for neutralized film prepared form dispersion with pH4 (film nCS/$Mg(OH)_2$_pH4, Fig. 1b). SEM images (Fig. 1, right column) depict the μ-scale, topographic features of the films. Random presence of micro-voids between well defined, discrete, as well as merged spherical particles were observed within neat CS films (Fig. 1b, top). These irregularities disturb the propagation of light, causing film opacity. Those features are the consequence of polymer de-solvation when polymer–polymer hydrophobic interactions and hydrogen bonding (Cho et al. 2006) dominates over the repulsive forces among protonated amines. Indeed, regardless of the solid form (powder, flakes, etc.), the CS chains are tightly packed due to the intrinsic tendency of the polymer to aggregate through van der Waals forces inherent to functional groups in its molecular structure. Even in a slightly acidic medium, although some chains may be solvated, the vast majority are expected to still form packaged insoluble structures (aggregates) whose ionized amine groups are present in a high fraction on their surfaces (Giraldo and Rivas 2021). Moreover, the presence of Cl^- counterions from the CS solvent (HCl) can impair the long-range organization within the CS molecules by immobilizing the hydration water, which is an additional cause of of″defects″(voids) formation within the structure (Gartner et al. 2011). In the dry state, $MgCl_2$ can be assumed to be present.

The addition of $Mg(OH)_2$ makes the films much more homogeneous and voids-absent. According to a study of Liu et al. (Wetteland et al. 2018), the Cl^- bind to the intermediate $MgOH^+$ formed during $Mg(OH)_2$ dissociation, which decreases the adsorption of H^+ to nearby $Mg(OH)_2$, and further enhance dissociation of $Mg(OH)_2$. The released OH^- allows stepwise neutralization of CS, which reduces the formation of aggregates and voids between them. Further addition of $Mg(OH)_2$ within the system with higher alkalinity (reaching the pH 6) do not follow the same trend as particles become much less soluble, and remain within dry films in particulate form, randomly distributed within the films (Fig. 1c). This observation discourages the future addition of $Mg(OH)_2$, meaning the films did not overpass the pI of CS ∼ pH 6.5 and remain soluble. To omit their gelling and decomposition, the neutralization with 1 M NaOH was performed. The most pronounced effect in terms of microstructure was observed in the neat CS film, where complete disappearance of voids, the particles fusion and film flattening were observed, most probably due to re-organization of CS molecules, leading to a more compact structure (Takara et al. 2015).

The same was further confirmed at the nanoscale, within AFM micrographs on Fig. 2. Herein, the neat CS film demonstrates the presence of large "islands"

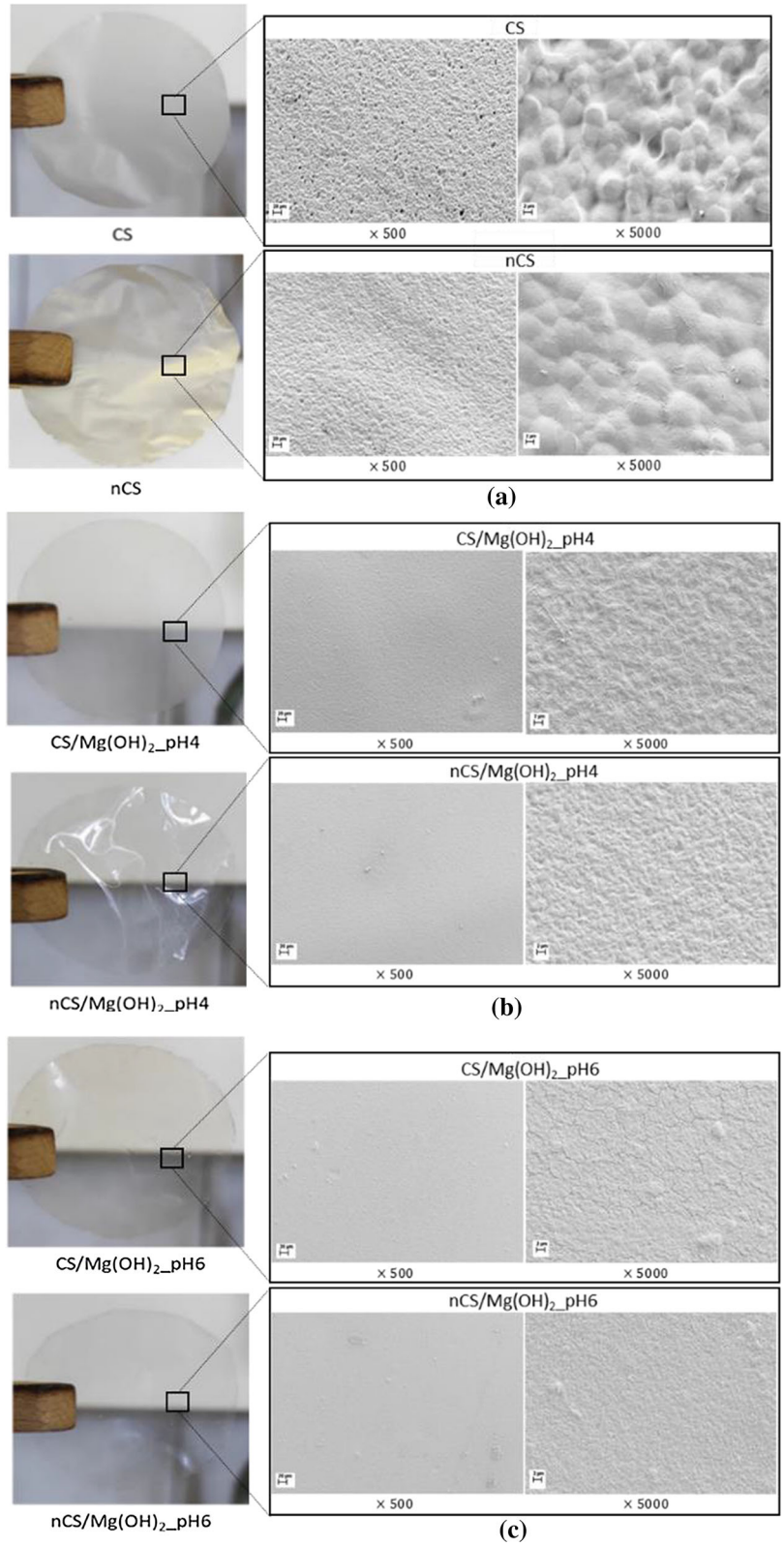

Fig. 1 **a** Photographs and different magnification SEM micrographs of **a** CS and CS/$Mg(OH)_2$ films, the latter prepared at **b** pH 4 and **c** pH 6, before and after neutralization with 1 M NaOH (prefix n stands for films neutralized with 1 M NaOH)

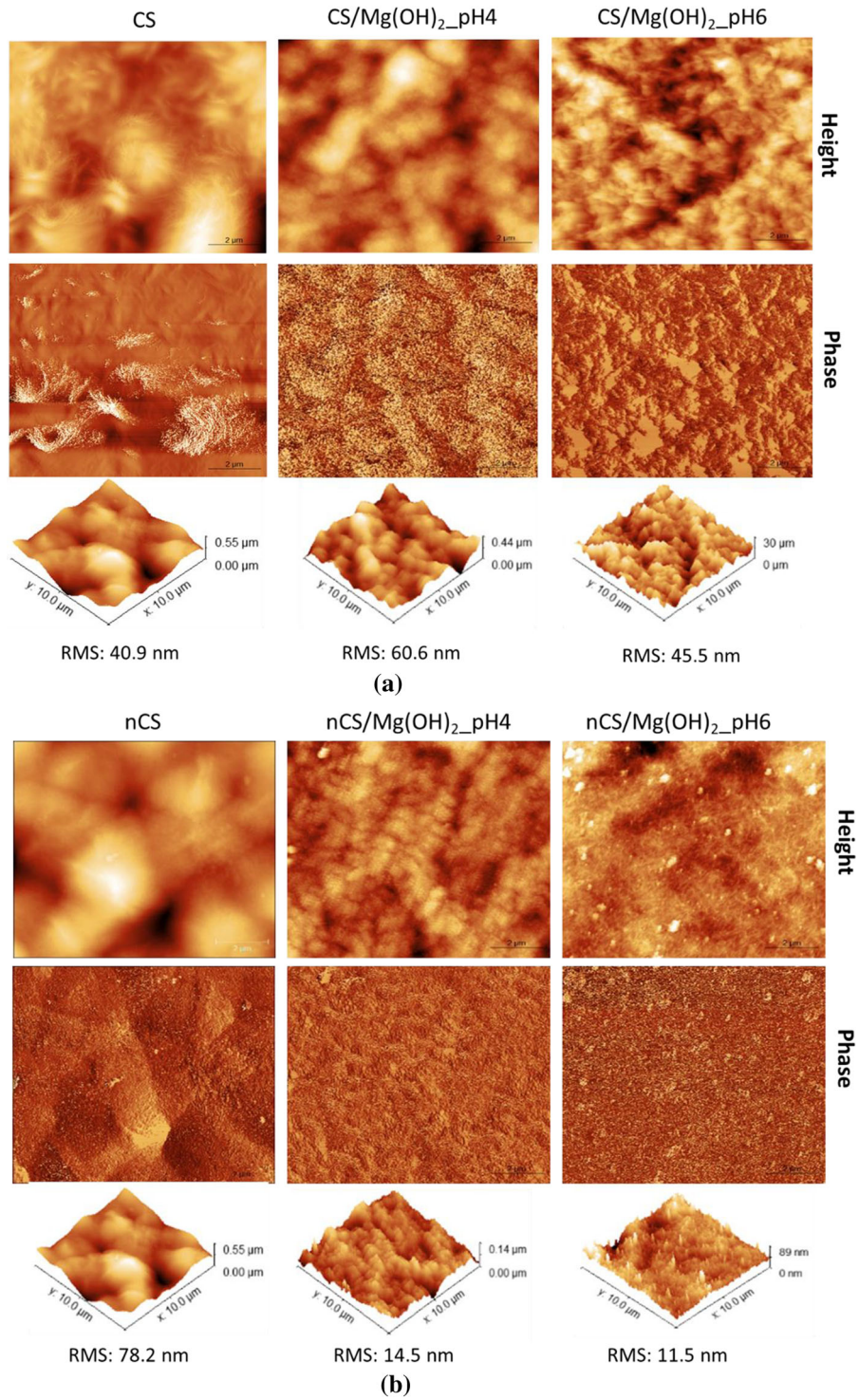

Fig. 2 AFM height, phase and 3D images of neat CS films at pH 2 and CS/$Mg(OH)_2$_pH4 and CS/$Mg(OH)_2$_pH6 composite films **a** before and **b** after neutralization with 1 M NaOH

or "particle-like features with roughness values of approximately 41 nm, when examined on 10 × 10 μm^2 areas. These features were less pronounced in the neutralized CS film, yet, in both cases, relatively high RMS values were found. There were differences in surface morphology and roughness for CS film after the addition of alkaline $Mg(OH)_2$ nanoparticles. Although the addition of $Mg(OH)_2$ still exhibited a roughness similar to that of the neat CS film before treatment, the uniformity of the surface of the latter film was improved, which goes ahead with the assumption for step-wise deprotonation, restricting the CS aggregation. After neutralization with 1 M NaOH, the film surfaces became rather smoother with a lower (15 nm) RMS value, confirming the SEM observation, also on the nanoscale. Overall, the surface roughness decreases in order CS > CS/$Mg(OH)_2$_pH4 > CS/$Mg(OH)_2$_pH6, as well as after neutralization with 1 M NaOH, while the opposite holds for homogeneity of the films. The lowest RMS value (11.5 nm), find for nCS/$Mg(OH)_2$_pH6 can be explained by the appearance of nanoparticles after neutralization 1 M NaOH, where we speculate the precipitation of $Mg(OH)_2$ from $MgCl_2$ due to exposure in highly basic media. The fact that they resist the intensive washing process indicates that these particles are well embedded into the film's structure.

Chemical characterization

The FTIR spectroscopy was used to assess the CS-CS and CS-$Mg(OH)_2$ interactions, before and after neutralization with 1 M NaOH. Figure 3 the asymmetric broadband in the range between 3000 and 3700 cm^{-1} can be attributed to O–H stretching vibrations in CS. Within this region, the neat CS membrane exhibited three well-defined peaks at 3450 cm^{-1}, 3362 cm^{-1}, and 3310 cm^{-1}, indicating the presence of free OH groups, the N−H stretching and H-bonded O−H stretch vibrational frequencies, respectively. Next are vibrations a $\sim$ 2980 cm^{-1}, ascribed to the stretching of saturated C−H groups. The higher intensity peak at 2863 cm^{-1} and the lower intensity peak at 2915 cm^{-1}, in the C−H stretch region of the spectra, are characteristic of the symmetric and asymmetric modes of CH_2 group vibrations, respectively, the latter appearing only in case of films neutralized with 1 M NaOH. This is an indication of the change in orientation of acetylated groups, which, as can be seen later one affect the hydrophilicity/hydrophobicity character of the film's surface. We speculate on possible outwards exposure of hydrophobic (-CH_2) moiety; the same will affect the contact angle data, described in the following section.

Other characteristic peaks for CS, observed at 1651 cm^{-1} (C = O stretching vibration of the amide I group, 1580 cm^{-1} (N–H bending of NH_2), 1420 cm^{-1} and 1380 cm^{-1} (CH_2 deformation and CH_3 symmetrical deformation in the residual amide N-acetyl group, respectively) and 1320 cm^{-1} (amide III, CH_2 wagging). Most intensive changes were observed in the position of amide I and II regions were shifting towards higher wavenumbers, was seen from $\sim$ 1620 to $\sim$ 1650 cm^{-1} for amide I and $\sim$ 1520 cm^{-1} to 1580 cm^{-1} in amide II, due to change in conformation of amide moiety and deprotonation of amine group after neutralization NaOH, respectively. Both changes are closely related as deprotonation reduces the hydration shell of the amine groups and allowed new hydrogen bonds to form in the CS chains (Takara et al. 2015), thus a change in molecular conformation occurs to rebalance the total energy of the system.

Comparing the CS and CS/$Mg(OH)_2$ films, the main difference was a reduction of two peaks at 2915 cm^{-1} and 2863 cm^{-1} into one at 2875 cm^{-1} (indicate by black arrows), which can suggest on interactions of Mg^{2+} with the acetyl residues present on partially deacetylated CS. Moreover, in the composite film prepared at pH 6, the deprotonation-related shifting of the –NH_2 group was observed (shift from 1517 cm^{-1} in CS to 1512.6 cm^{-1} in CS/$Mg(OH)_2$_-pH6) confirming the neutralization of $Mg(OH)_2$. The vibration of carbonyl bonds (C = O) in amide group CONHR was also affected by $Mg(OH)_2$ presence (shift from 1623.3 cm^{-1} in CS to 1647.5 cm^{-1} in CS/$Mg(OH)_2$_pH6).

The absorption band at 1150 cm^{-1} pertains to the asymmetrical stretching of the C−O−C bridge, and the skeletal vibration involving C−O stretching at 1029 cm^{-1}. Both are characteristically assigned to the CS saccharide structure. No change in position and intensity was observed for C–O–C bridge vibration after the neutralization process, while the latter cause shifting in the C–O region, again suggesting conformation change, as described previously.

Importantly, the strong vibration at 3695 cm^{-1} in $Mg(OH)_2$ powder spectra, assigned to the OH groups on the surface, at the edge, or in the corner sites of

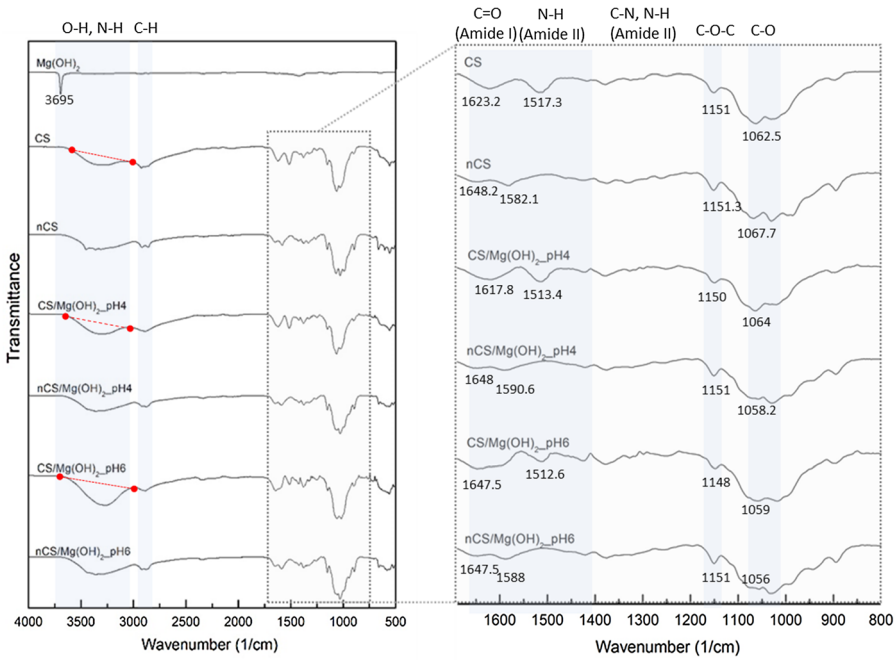

Fig. 3 ATR-FTIR spectral lines of CS and CS/$Mg(OH)_2$ films, the latter prepared at pH 4 and pH 6, before and after neutralization with 1 M NaOH (prefix n stands for films neutralized with 1 M NaOH)

nanoparticles (Kurosawa et al. 2021) is absent in CS/$Mg(OH)_2$ films. A close look after the surface of the broad O–H bonding-related region in CS/$Mg(OH)_2$ films (area below red, dotted lines) demonstrate enlargement of this vibration. Both findings strongly suggest on absence and dissolution of these nanoparticles in non-integrated form and intensive H-bonding interaction between CS and nanoparticles.

XPS was further used to identify the chemical composition of respective films and to investigate the interactions among film components, before and after neutralization. Quantitative chemical data of films are shown in Table 1. Neat CS films contain chloride ions from the HCl dissolution and show a significantly higher carbon and lower nitrogen and oxygen content than theoretically expected for pure CS. For CS films containing $Mg(OH)_2$ (pH 4 and pH 6, before neutralisation with 1 M NaOH) %C and %Mg increased, while %O, %N and %Cl atoms decreased, comparing to neat CS. The increase of %C (C 1 s peak at 285.0 eV) can be assigned to the low amount of $MgCO_3$ product that is formed between $Mg(OH)_2$ and CO_2 in the air (Yap et al. 2011), which was not detected by FTIR due to low concentrations. Cl^- is a counterion from CS solvent (the HCl), which can bind and stabilise the intermediate $MgOH^+$ formed during $Mg(OH)_2$ dissociation and $MgCl_2$ formation. Consequently, the concentration of Cl^- was reduced with an increase of pH, while the same was completely removed after the neutralisation process when $Mg(OH)_2$ was re-precipitated, and Cl- washed away from the films. On the other hand, there is no obvious change in %Mg after neutralisation, confirming strong interaction with CS moieties and probably the reformation of $Mg(OH)_2$. Surface nitrogen decreases concomitantly with an increase in carbon content which can be interpreted as partial deamination through elimination by the harsh chemical treatments.

Table 1 Surface composition of the CS-based films (in at%)

	C	N	O	Mg	Cl
CS_{theor}	54.5	9.0	36.4	/	/
CS	66.5	4.9	24.0	0	4.0
CS/$Mg(OH)_2$_pH4	69.3	3.9	21.5	0.6	3.2
CS/$Mg(OH)_2$_pH6	74.2	2.7	20.0	1.0	1.7
nCS	67.0	5.1	25.6	0	/
nCS/$Mg(OH)_2$_pH4	68.7	4.0	25.5	0.9	/
nCS/$Mg(OH)_2$_pH6	70.3	3.9	23.2	1.1	/

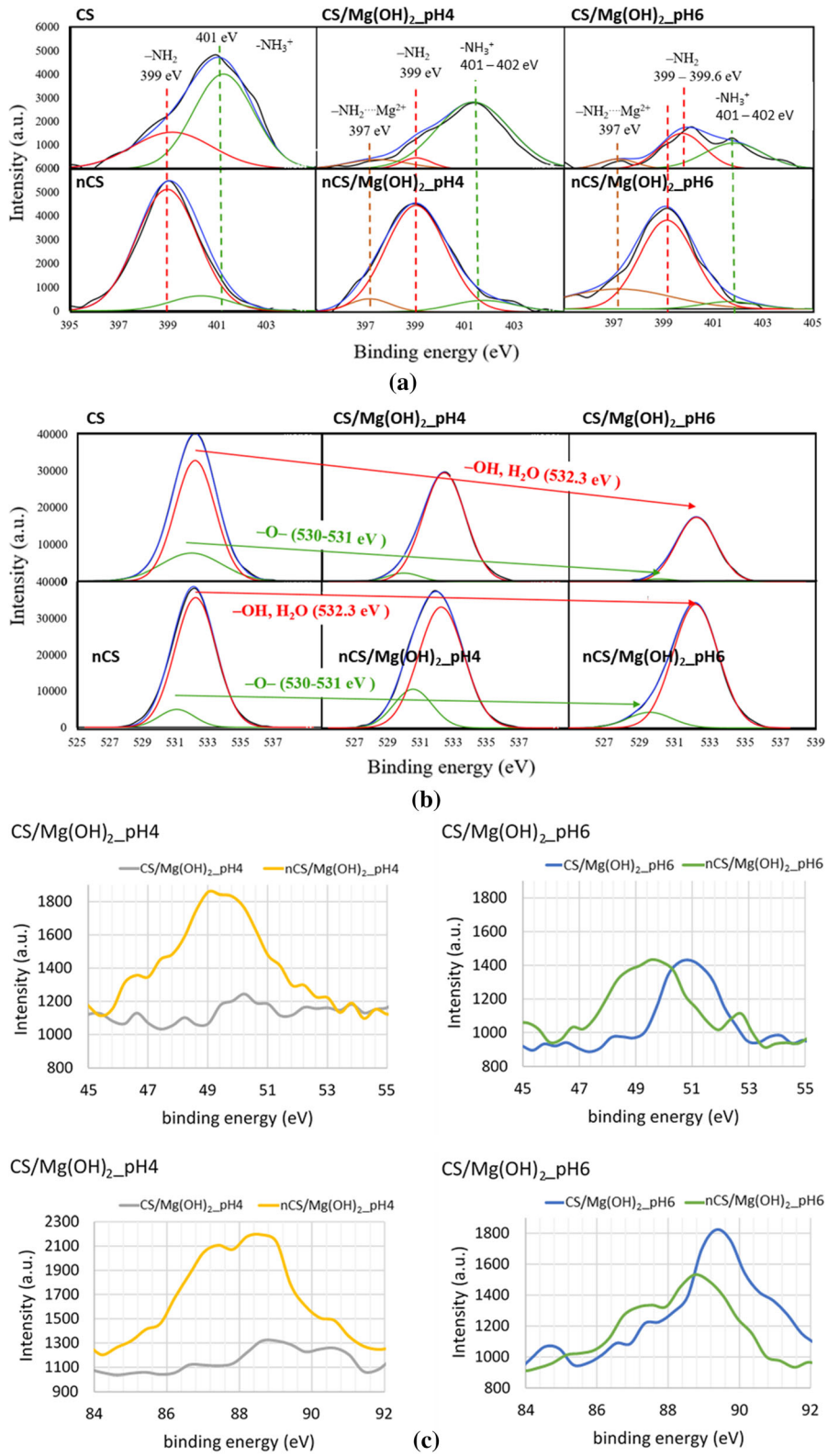

Fig. 4 **a** N1s, **b** O1s and **c** Mg2p XPS spectra of CS films at pH 2 and CS/$Mg(OH)_2$ composite films at pH 4 and pH 6 before and after neutralization

The high-resolution N1s XPS spectra of CS and CS/$Mg(OH)_2$ films are shown in Fig. 4a. There are two N1s peaks located at 399 eV and 401–402 eV for neat CS film, which are attributed to the existence of the nitrogen atoms in the $–NH_2$ and $–NH_3^+$ groups, respectively (Yap et al. 2011; Shen et al. 2013). After mixing of $Mg(OH)_2$ nanoparticles with acidic CS solution, the formed films evidence the same two peaks, where overall N1s peak intensity decreased with increasing the $Mg(OH)_2$ concentration, indicating possibly deamination and a dilution effect of the salt. A new band around 397 eV was found in the spectrum of CS/$Mg(OH)_2$ films at pH 4 and pH 6, being attributed to the interaction between $–NH_2$ group and free Mg^{2+} ions released from $Mg(OH)_2$ nanoparticle due to partial dissolution. The overall peak intensity of $–NH_3^+$ groups decreased from pH 2 to pH 6 before and after neutralization, being accompanied by the deprotonation of $–NH_3^+$ induced by the added $Mg(OH)_2$, and immersion in 1 M NaOH. Due to deprotonation of $–NH_3^+$, the peak intensity of $–NH_2$ increased, especially after films neutralization with NaOH.

For the spectrum of O1s (Fig. 4b), the band of the neat CS film was composed of two sub-bands, which are attributed to the existence of R-OH, or bound H_2O (532.3 eV) and the –O– in the ring and possibly –O– between the rings (530 – 531 eV) which exist in CS structure (Rashid et al. 2015). After neutralisation, no significant difference was observed among the O1s spectrum of different films.

The spectrum at Fig. 4c showed two additional peaks at around 89 eV and 51 eV, assigned to Mg_{2s} and Mg_{2p}, respectively. The Mg2p level is close to the valence band and, therefore, it is easy to observe changes in the valence band and to identify the valence state for this element. In this case, a shift to higher binding energies occurs when a valence electron is lost because the bonds become stronger, i.e., anions have lower binding energies than atoms. Therefore, for the Mg2p peaks, it is inferred that the peak at higher binding energy is related to $MgCO_3$ or dioxygen species, such as MgO_2. The specimens present an additional peak at approximately 49–50 eV which is attributed to $MgCl_2$ and 51.4 eV, which is associated with crystalline $Mg(OH)_2$, that might be reformed during neutralization with NaOH and subsequent washing which was observed in traces with SEM micrographs.

Contact angle (CA) data

Figure 5 demonstrate absorption of water droplets captured at a different time until complete drop disappearance, and respective CA values (°) for films, before and after neutralization with 1 M NaOH. After 60 s, the CA was around 60° for CS film, 80° for CS/$Mg(OH)_2$_pH4 film and 90° for CS/$Mg(OH)_2$_pH6 film. Moreover, the rate of droplet deformation and disappearance from film surface decrease by CA increment, and drop remain longest on CS/$Mg(OH)_2$_-pH6 films, i.e. 6 and 8 min, without and with film neutralization, respectively. The same indicates that the addition of $Mg(OH)_2$, as well as neutralization with 1 M NaOH, reduce the hydrophilicity, probably due to re-packaging of CS polymer chains at neutralization, as already traced by FTIR as increment in hydrophobic moiety vibrations. Another important factor which reduces the contact angle and resistance of droplet onto the film is the surface roughness and presence of voids, which were observed in CS films. Nonetheless, the same trend remains after the neutralization with 1 M NaOH (i.e. lowest angles measure in CS films), when voids were not present and membranes were significantly flattened, which eliminate the surface roughness factor on CA.

Crystallinity

XRD patterns of CS and CS/$Mg(OH)_2$ films, before and after neutralization with 1 M NaOH are present in Fig. 6. CS and CS/$Mg(OH)_2$_pH 4 films showed peaks between 10° and 12° and between 23° and 25° being typical fingerprints of semicrystalline CS, corresponding to hydrated and anhydrous crystal structures of CS, respectively (Ogawa et al. 2004). Additional shoulder $\sim$ 10° in CS/$Mg(OH)_2$_pH 6 may indicate interaction of CS (the hydrated crystals) with $Mg(OH)_2$, introducing a higher degree of crystallinity within the film (Mohanasrinivasan et al. 2014). Indeed, the typical crystalline peaks for $Mg(OH)_2$ were not observable at 38° (101), 51° (102) and 58° (110), which suggest dissolution of $Mg(OH)_2$ nanoparticles and their re-precipitation within the film, as demonstrated by FTIR, which cause rearrangement and even increase in overall crystallinity of the system, from 52.1% in CS to 62.6% in CS/$Mg(OH)_2$_pH6.

After neutralization with 1 M NaOH, we can observe a significant increment in film crystallinity.

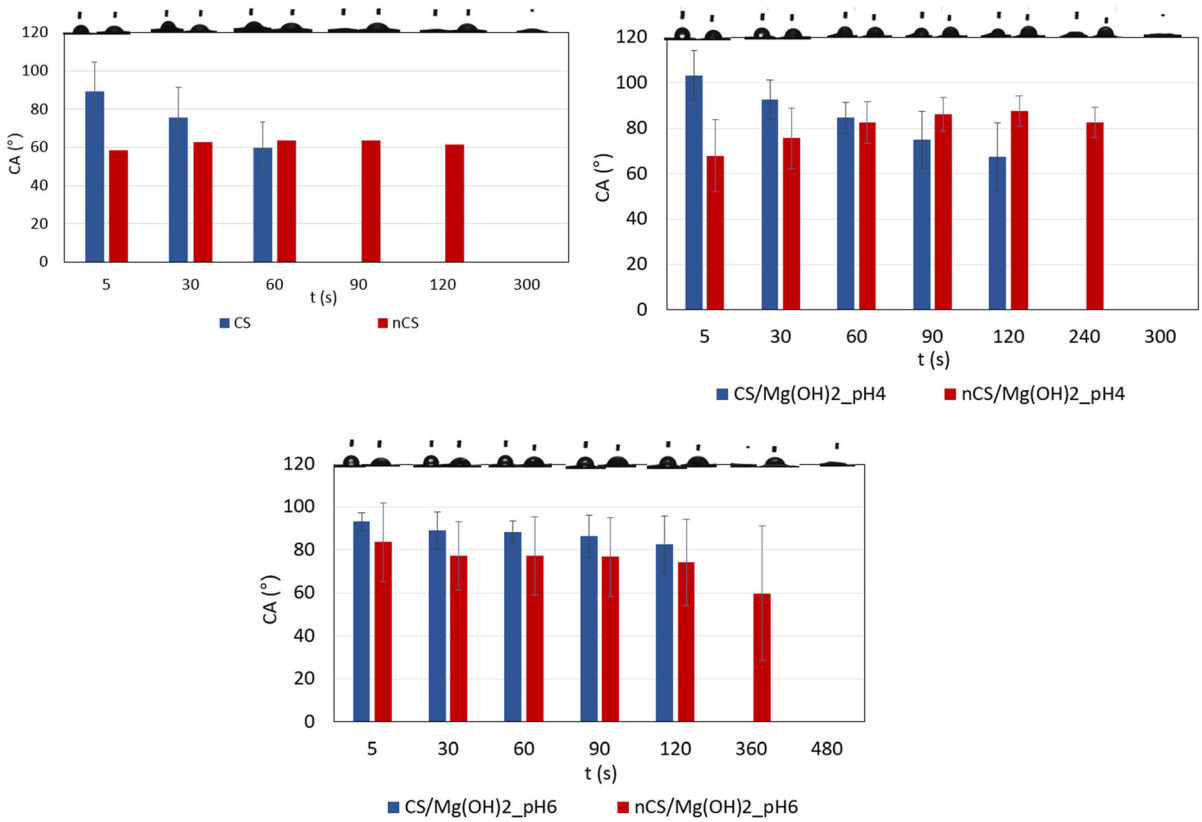

Fig. 5 Contact angle data and respective images for neat CS films at pH 2 and CS/$Mg(OH)_2$ composite films at pH 4 and pH 6, measured before and after neutralization with 1 M NaOH. Data were taken at time intervals, starting from 5 s up to complete water drop adsorption within the film

By NaOH neutralized CS and CS/$Mg(OH)_2$_pH4 films showed the high intensity of diffraction peaks around 2θ = 10°, 15°, and 20° with the small shoulder at 2θ = 23°. Peaks at 2θ = 10° and 20° correspond to CS crystal I and crystal II structure, whereas the peak at 2θ = 15° indicated on anhydrous polymorph in CS films. The most intense crystallinity peaks at 2θ = 10°, 19° and 20°, with almost no peak at 15° were obtained for CS film prepared from CS solution of pH 6.0 after neutralization with 1 M NaOH.

In line with results by Takara (2015), two hydrated and anhydrous polymorphs can be identified with CS films after treatment with NaOH. The latter cause re-packing of CS polymer chains into more regular structure and formation of the new hydrogen links. Presence of $Mg(OH)_2$ in higher quantity (pH6) has obvious contribution in crystal patterns, supporting formation of hydrated polymorph, while diminishing the anhydrous polymorph formation.

Oxygen transmission rate (OTR) and oxygen permeability (OP)

When application as packaging materials is considered, the oxygen transmission rate and oxygen permeability are very crucial parameters, due to the detrimental effect of oxygen on the food quality and their shelf life. As can be seen within Table 2, the OTR and OP values were significantly reduced by $Mg(OH)_2$ addition, as well neutralization with 1 M NaOH. OTR values of films before neutralization decline from 5300 cm^3 m^{-2} day^{-1} in neat CS, down to 7 cm^3 - m^{-2} day^{-1} at in CS/$Mg(OH)_2$_pH6. The same trend was seen in OP data. The neutralization with 1 M NaOH even further reduced both parameters, most probably due to the higher crystallinity, which hinders the diffusion of oxygen molecules through the film. Indeed, the diffusion energy required for gas to pass through the high crystallinity film is higher than that of the low crystallinity or non-crystallinity film, and the

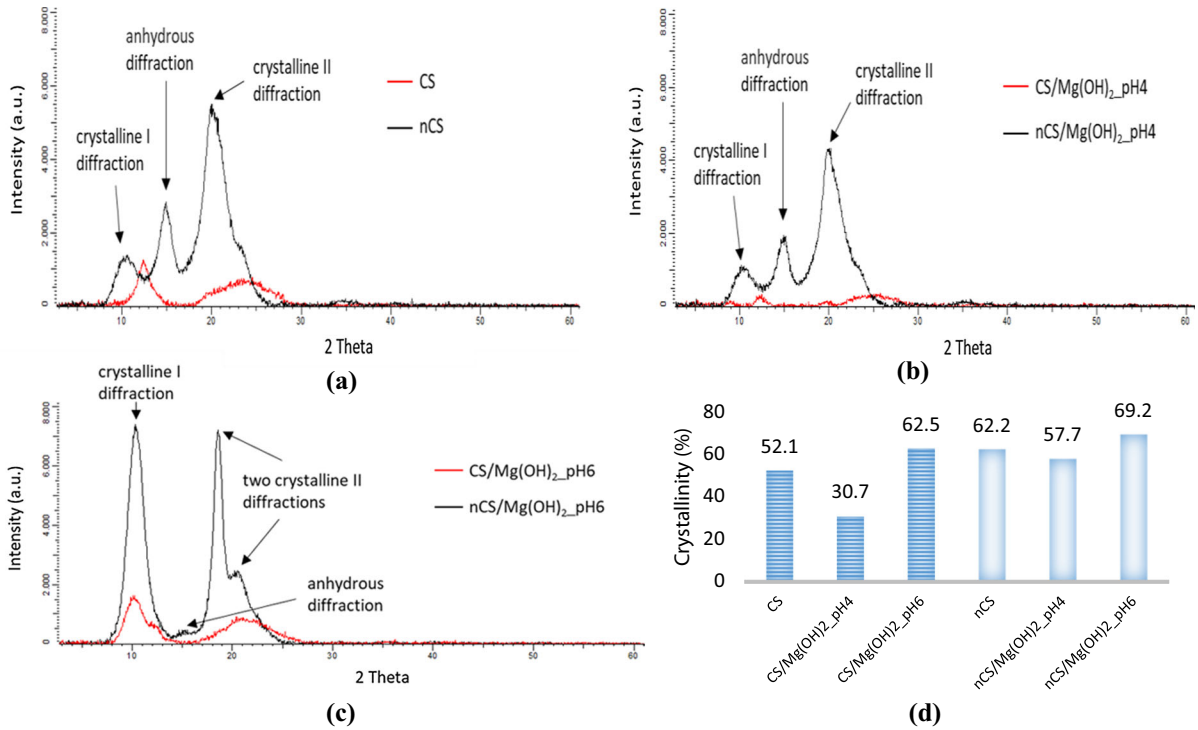

Fig. 6 X-ray diffractograms of **a** CS, **b** CS/$Mg(OH)_2$_pH4, **c** CS/$Mg(OH)_2$_pH6 films, before and after neutralization with 1 M NaOH and **d** b) % crystallinity calculated by dividing the area of the crystalline peaks by the total area under the curve from 2θ 5° to 30°

Table 2 Oxygen transmission rate (OTR) and oxygen permeability (OP) of CS films at pH 2, 4 and 6 before and after neutralization with 1 M NaOH

Sample	OTR (cm^3 m^{-2} day^{-1})	OP (cm^3 µm m^{-2} day^{-1} atm^{-1})
CS	5 313 ± 710	192 841 ± 11 484
nCS	1 059 ± 319	37 670 ± 15 000
CS/$Mg(OH)_2$_pH 4	1 854 ± 937	67 470 ± 29 476
nCS/$Mg(OH)_2$_pH 4	294 ± 103	11 086 ± 2918
CS/$Mg(OH)_2$_pH 6	7 ± 1	287 ± 43
nCS/$Mg(OH)_2$_pH 6	141 ± 44	5 801 ± 2248

diffusion coefficient was small, so it showed a better gas resistance (Liu et al. 2020). Prepared CS/$Mg(OH)_2$ composite films demonstrate a very high barrier to oxygen, and excellent performance, especially when comparing to commercial synthetic polymers (OP of polypropylene is 50 000–100 000 cm^3 µm m^{-2} - day^{-1} atm^{-1}, polyethylene is 50 000–200 000 cm^3 - µm m^{-2} day^{-1} atm^{-1}, polyethylene terephthalate 1000–5000 cm^3 µm m^{-2} day^{-1} atm^{-1}) (Wang et al. 2018).

Water vapour permeability (WVP)

The reduction of moisture transfer between the food and the surrounding atmosphere, or between two components of a heterogeneous food product is desirable, and low WVP is appropriate for food packaging films (Adjouman et al. 2017). Figure 7 display WVP data for the films library, at 50% and 64% relative humidity (RH). At higher RH, the permeability of films was lower, which maid be the consequence of hydration of films, closing the pores

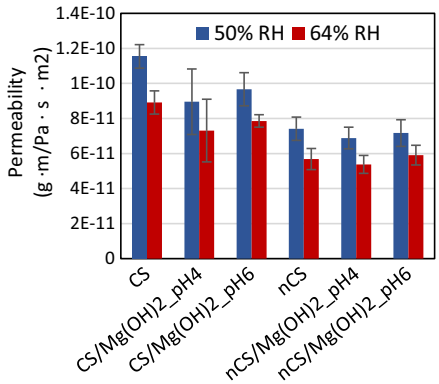

Fig. 7 Water vapour permeability (WVP) value for CS films at pH 2, 4 and 6 before and after neutralization with 1 M NaOH

and reducing the permeation of vapour. Nevertheless, we can observe the same trend at both, 50% and 64% RH—decreasing WVP after neutralization with 1 M NaOH, while a very small difference was observed in CS/$Mg(OH)_2$_pH 6 film, comparing to neat, CS film. Measured values are in the range or even better than reported values for certain biodegradable plasticized films, such as corn starch plasticized with sorbitol (Garcia et al. 2000), and even some synthetic films, such as cellophane (8.4×10^{-10} g·m/Pa s m^2), but higher than low-density polyethylene and high-density polyethylene, which have $\sim$ 2 orders of magnitude lower values as an excellent water vapour barrier films. The values are also low compared to certain emulsified films, for example, hydroxypropyl methylcellulose with plasticizer and oil, cassava starch and 15% glycerol with hydrogenated vegetable oil, and agar, 15% glycerol and hydrogenated vegetable oil, etc (Adjouman et al. 2017).

Due to the presence of hydrophilic domains of CS film, the water vapour was more easily absorbed, and the diffusion step was improved substantially (Liu et al. 2020). Lack of plasticizers positively contributes to water vapour permeability of films, as the hydrophilic nature of these components usually eases the water vapour diffusion, increasing the water vapour permeability concerning pure CS films (Cazón and Vázquez 2020). Packaging films should maintain moisture levels within the packaged product. Therefore, the knowledge of moisture content is another important parameter for food packaging applications (Wang et al. 2011). Table 3 insert within Fig. 7 display moisture content of CS films, indicating similar values for films before neutralization at different pH, being around 20%. The films treated with 1 M NaOH demonstrate the superior resistance to moisture than films before treatment, irrespective of pH, again, as a consequence of increased crystallinity, as well as surface groups orientation.

Table 3 Moisture content of CS-based films at 20 °C and 64% RH

Sample	Moisture content (%)
CS	20.65 ± 0.27
nCS	12.80 ± 0.13
CS/$Mg(OH)_2$_pH4	20.94 ± 0.50
nCS/$Mg(OH)_2$_pH4	13.23 ± 0.59
CS/$Mg(OH)_2$_pH6	22.47 ± 2.09
nCS/$Mg(OH)_2$_pH6	13.04 ± 0.49

Mechanical properties

Mechanical properties of CS film are closely related to DD and M_W of polymer, CS percentage at preparation, solvent, drying temperature (Homez-Jara et al. 2018), etc. Herein, we exclude any addition of plasticizer, or crosslinker and monitor the effect of $Mg(OH)_2$ addition and neutralization with 1 M NaOH on the mechanical response of the films under tensile test.

The values of elastic modulus, tensile strength, and elongation at break for different CS films are shown in Table 4. These results indicated that elastic modulus increased after neutralization with 1 M NaOH in all films, causing film brittleness, where the most brittle film was CS/$Mg(OH)_2$_pH6, having twice higher E-modulus (around 12 MPa) than neat CS film. This result goes ahead with an increase of crystallinity, following the same trend. Oppositely, tensile strength and elongation at break decreased after neutralization due to decreased flexibility of the films. This was not the case only for films with the highest tensile strength and elongation at break (CS/$Mg(OH)_2$_pH4), which even improve after neutralization (nCS/$Mg(OH)_2$_-pH4), suggesting on strong interaction among CS groups and $Mg(OH)_2$ in this combination. Results are in correlation with SEM observation, where the structural integrity of the films was observed after the addition of the $Mg(OH)_2$. The addition of higher content of $Mg(OH)_2$ do not further improve, but only contribute to discussed film brittleness as the system

Table 4 Mean of elastic modulus, tensile strength and elongation at break for CS films prepared at different pH

Sample	E-Modulus (MPa)	Tensile strength (max.) (MPa)	Elongation at break (%)
CS	5.52 ± 0.60	0.86 ± 0.24	2.72 ± 0.75
nCS	9.26 ± 1.24	0.52 ± 0.15	1.66 ± 0.51
CS/$Mg(OH)_2$_pH4	4.70 ± 0.66	1.20 ± 0.69	3.88 ± 2.13
nCS/$Mg(OH)_2$_pH4	7.90 ± 2.11	1.54 ± 0.48	4.88 ± 1.48
CS/$Mg(OH)_2$_pH6	5.46 ± 2.14	1.16 ± 0.46	3.78 ± 1.48
nCS/$Mg(OH)_2$_pH6	11.92 ± 1.71	0.58 ± 0.12	1.9 ± 0.33

become overdosed by $Mg(OH)_2$ particles, to the extent when precipitates were observed.

Thermal properties

Differential scanning calorimetry (DSC) and thermogravimetric analysis (TGA) are complementary tools, used for demonstration of changes in thermal stability by the inclusion of $Mg(OH)_2$ and neutralization with 1 M NaOH. Figure 8a,b summarize the parameters of two main thermal transitions, extracted from thermograms, i.e. temperature of transition (main peak, °C), with respective energy (mJ/mg) and weight loss (%). The first, endotherm related to the evaporation of absorbed water, vary between 80 and 100 °C among films (Fig. 8a). A significant difference of energy used for this transition was observed, reducing with pH increase in films without subsequent neutralization. This is an indication of the reduced amount of adsorbed water due to increased hydrophobicity, as already demonstrated by contact angle measurement, as well as WVP data. This trend has vanished in films treated with 1 M NaOH, which was not the case with the second, exotherm transition related to degradation. The latter comes from the split of the glycoside bonds and decomposition of amine residues and occurs

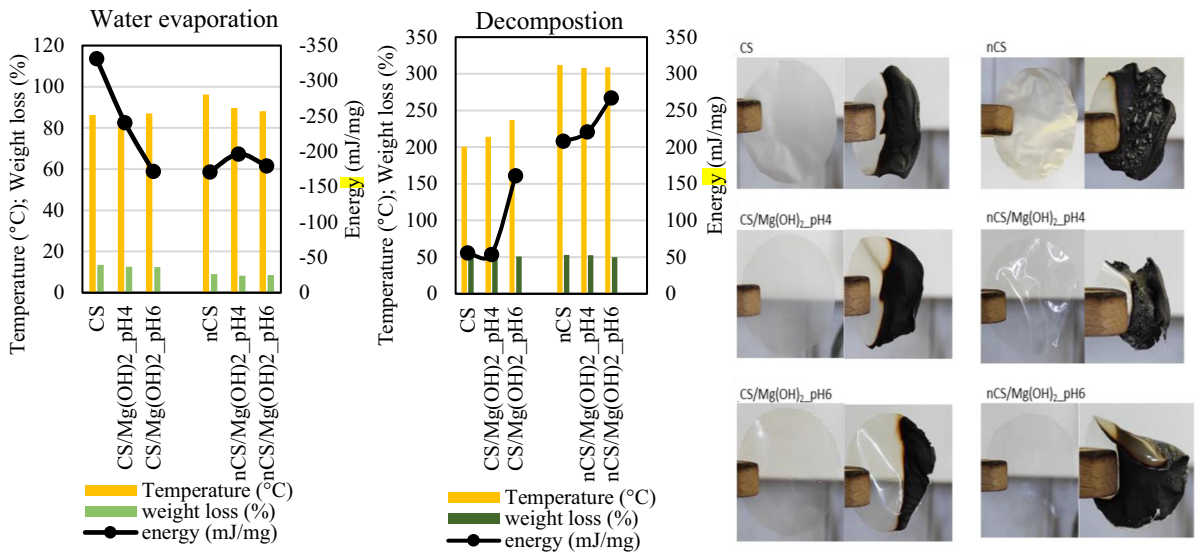

Fig. 8 Data (temperature, % weight loss and energy) extracted from DSC and TGA thermograms of neat CS films at pH 2 and CS/$Mg(OH)_2$ composite films at pH 4 and pH 6 before and after neutralization, related to **a** water evaporation thermal transition and **b** decomposition. **c** Digital photography presenting films before (left) and after (right) horizontal burning test. Films were held in the vertical position using wooden clamps and ignited endwise for 10 s. with a constant, 3 cm distance between butane burner and film

between 200 and 250 °C (Fig. 8b). Degradation temperature shifts to higher values with $Mg(OH)_2$ addition, while keeping constant after neutralization with 1 M NaOH. Even so, the energy of exotherm transition was higher in both cases, indicating improved thermal stability, where more energy is required to completely decompose films, especially in sample nCS/$Mg(OH)_2$_pH6.

To have a look at the behaviour of the films when they are exposed to open flame, the photographs were taken according to the procedure adapted from (Gorgieva et al. 2020). As can be seen from photographs in Fig. 8c, the chair formation was observed in all films and almost complete charring was demonstrated by 1 M NaOH- treated films. Besides, the presence of $Mg(OH)_2$, even small, demonstrate a reduction of burning, especially in the case of a film with higher content of this agent. In neat CS films, half of the membrane was burned, while $Mg(OH)_2$ presence reduce the burned surface to 1/3, evidencing a self-extinguishing behaviour. $Mg(OH)_2$ is a known flame retardant agent, which decomposes endothermically when heated, and the gaseous water phase is believed to envelop the flame, thereby excluding oxygen and diluting flammable gases, also forming the heat insulating material on the surface of the film reducing the flow of potentially flammable decomposition products to the gas phase where combustion occurs. It can be assumed that $Mg(OH)_2$ contributes to thermal stabilization of films, while additional treatment with 1 M NaOH only progresses the degradation of films by charring.

Conclusion

Aqueous acidic—CS solutions can be efficiently neutralized by the addition of alkaline $Mg(OH)_2$ nanoparticles, without causing inhomogeneous gelation of the polymer. This is not possible by the quick addition of NaOH to CS solutions where heterogeneous gelation occurs that cannot be redissolved during the process. This method, therefore, offers the possibility to adjust the pH value of the CS solutions before casting into sheets by drying. This allows for controlled deprotonation of the primary nitrogen present on the polymer and the simultaneous formation of magnesium chloride salt. There are particular differences in the properties of films that are cast from solutions comprising different pH values. Acidic CS solutions are relatively non-transparent whereas films cast from higher pH values are less opaque. More importantly, films cast at higher pH values show very significantly lower oxygen transmission rates in the dry state (OTR 7 ± 1 $cm^3\ m^{-2}\ day^{-1}$) far below standard synthetic packaging materials. This is attributed to either the efficient embedding of the nanoparticles into the polymer acting as an additional barrier material, or to a tighter packing of the polymer chains due to deprotonation of the nitrogen before film formation. X-ray scattering data also suggests a higher crystallinity of the filled and neutralized films, whereas also wetting and water content are lower for those that are less protonated. Films prepared by this method can in addition be neutralized by NaOH solutions after drying. This leads most likely to the reformation of $Mg(OH)_2$ from the $MgCl_2$ present initially as confirmed by X-ray photoelectron spectroscopy. It however does not reduce OTR values. Neutralization however reduces water vapour permeability. The methods presented here allow fine-tuning the precipitation of CS from solution and more sophisticated versions of such approaches might lead to nanocomposites with even higher-order and unexpected properties.

Funding The Financial support was received from the Slovenian Research Agency Young Researcher Program (P2-0118/0795), the project »Graphene Oxide-based MEAS for the Direct Ethanol Fuel Cell« (Grant Number N2-0087) and the Textile Chemistry Program (P2-0118).

Availability of data and material Data available from the author on the request.

Declarations

Conflict of interests The authors declare that they have no conflict of interest.

Consent for publication All authors agreed to the publication in the submitted form.

References

Abdou ES, Nagy KSA, Elsabee MZ (2008) Extraction and characterization of chitin and chitosan from local sources. Bioresour Technol 99:1359–1367. https://doi.org/10.1016/J.BIORTECH.2007.01.051

Adjouman YD, Nindjin C, Tetchi FA et al (2017) Water vapor permeability of edible films based on improved cassava (manihot esculenta crantz) native starches. J Food Process Technol 8:665. https://doi.org/10.4172/2157-7110.1000665

Bandara S, Du H, Carson L et al (2020) Agricultural and biomedical applications of chitosan-based nanomaterials. Nanomaterials 10:1–31

Božič M, Gorgieva S, Kokol V (2011) Laccase-mediated functionalization of chitosan by caffeic and gallic acids for modulating antioxidant and antimicrobial properties. Carbohydr Polym 87:2388–2398. https://doi.org/10.1016/j.carbpol.2011.11.006

Božič M, Gorgieva S, Kokol V (2012) Homogeneous and heterogeneous methods for laccase-mediated functionalization of chitosan by tannic acid and quercetin. Carbohydr Polym 89:854–864. https://doi.org/10.1016/j.carbpol.2012.04.021

Cazón P, Vázquez M (2020) Mechanical and barrier properties of chitosan combined with other components as food packaging film. Environ Chem Lett 18:257–267

Cho J, Heuzey MC, Bégin A, Carreau PJ (2006) Viscoelastic properties of chitosan solutions: effect of concentration and ionic strength. J Food Eng 74:500–515. https://doi.org/10.1016/j.jfoodeng.2005.01.047

Cui J, Yu Z, Lau D (2016) Effect of acetyl group on mechanical properties of chitin/chitosan nanocrystal: a molecular dynamics study. Int J Mol Sci 17:1–13. https://doi.org/10.3390/ijms17010061

Cui L, Gao S, Song X et al (2018) Preparation and characterization of chitosan membranes. RSC Adv 8:28433–28439. https://doi.org/10.1039/c8ra05526b

Drevinskas T, Naujokaitytė G, Maruška A et al (2017) Effect of molecular weight of chitosan on the shelf life and other quality parameters of three different cultivars of Actinidia kolomikta (kiwifruit). Carbohydr Polym 173:269–275. https://doi.org/10.1016/j.carbpol.2017.06.002

Eivazzadeh-Keihan R, Radinekiyan F, Aliabadi HAM et al (2021) Chitosan hydrogel/silk fibroin/Mg(OH)2 nanobiocomposite as a novel scaffold with antimicrobial activity and improved mechanical properties. Sci Rep. https://doi.org/10.1038/s41598-020-80133-3

French AD (2020) Increment in evolution of cellulose crystallinity analysis. Cellulose 27:5445–5448

Garcia MA, Martino MN, Zaritzky NE (2000) Lipid addition to improve barrier properties of edible starch-based films and coatings. J Food Sci 65:941–944. https://doi.org/10.1111/j.1365-2621.2000.tb09397.x

Gartner C, Löpez BL, Sierra L et al (2011) Interplay between structure and dynamics in chitosan films investigated with solid-state NMR, dynamic mechanical analysis, and X-ray diffraction. Biomacromol 12:1380–1386. https://doi.org/10.1021/bm200193u

Giraldo JD, Rivas BL (2021) Direct ionization and solubility of chitosan in aqueous solutions with acetic acid. Polym Bull 78:1465–1488. https://doi.org/10.1007/s00289-020-03172-w

Gorgieva S, Kokol V (2012) Preparation, characterization, and in vitro enzymatic degradation of chitosan-gelatine hydrogel scaffolds as potential biomaterials. J Biomed Mater Res Part A 100:1655–1667. https://doi.org/10.1002/jbm.a.34106

Gorgieva S, Vuherer T, Kokol V (2018) Autofluorescence-aided assessment of integration and μ-structuring in chitosan/gelatin bilayer membranes with rapidly mineralized interface in relevance to guided tissue regeneration. Mater Sci Eng C 93:226–241. https://doi.org/10.1016/J.MSEC.2018.07.077

Gorgieva S, Jančič U, Hribernik S et al (2020) Processing and functional assessment of anisotropic cellulose nanofibril/Alolt/sodium silicate: based aerogels as flame retardant thermal insulators. Cellulose 27:1661–1683. https://doi.org/10.1007/s10570-019-02901-3

Gorgieva S, Osmić A, Hribernik S et al (2021) Efficient chitosan/nitrogen-doped reduced graphene oxide composite membranes for direct alkaline ethanol fuel cells. Int J Mol Sci. https://doi.org/10.3390/ijms22041740

Hejazi M, Behzad T, Heidarian P, Nasri-Nasrabadi B (2018) A study of the effects of acid, plasticizer, cross-linker, and extracted chitin nanofibers on the properties of chitosan biofilm. Compos Part A Appl Sci Manuf 109:221–231. https://doi.org/10.1016/j.compositesa.2018.02.038

Hirano S, Hirochi K, Hayashi K et al (1991) Cosmetic and Pharmaceutical Uses of Chitin and Chitosan. Cosmetic and Pharmaceutical Applications of Polymers. Springer, US, pp 95–104

Homez-Jara A, Daza LD, Aguirre DM et al (2018) Characterization of chitosan edible films obtained with various polymer concentrations and drying temperatures. Int J Biol Macromol 113:1233–1240. https://doi.org/10.1016/j.ijbiomac.2018.03.057

Hren M, Hribernik S, Gorgieva S et al (2021) Chitosan-Mg(OH)2 based composite membrane containing nitrogen doped GO for direct ethanol fuel cell. Cellulose 28:1599–1616. https://doi.org/10.1007/s10570-020-03603-x

Hu H, Yang L, Lin Z, et al (2018) A low-cost and environment friendly chitosan/aluminum hydroxide bead adsorbent for fluoride removal from aqueous solutions. Iran Polym J (English Ed) 27:253–261. https://doi.org/10.1007/s13726-018-0605-x

Kaker B, Hribernik S, Mohan T et al (2019) Novel Chitosan–Mg(OH) $_2$ -based nanocomposite membranes for direct alkaline ethanol fuel cells. ACS Sustain Chem Eng 7:19356–19368. https://doi.org/10.1021/acssuschemeng.9b02888

Kurosawa R, Takeuchi M, Ryu J (2021) Fourier-transform infrared analysis of the dehydration mechanism of Mg(OH) 2 and chemically modified Mg(OH) 2. J Phys Chem C 125:5559–5571. https://doi.org/10.1021/acs.jpcc.0c08696

Liu Y, Yuan Y, Duan S et al (2020) Preparation and characterization of chitosan films with three kinds of molecular weight for food packaging. Int J Biol Macromol 155:249–259. https://doi.org/10.1016/j.ijbiomac.2020.03.217

Manigandan V, Karthik R, Ramachandran S, Rajagopal S (2018) Chitosan applications in food industry. In: Biopolymers for food design. Elsevier, pp 469–491

Mauricio-Sánchez RA, Salazar R, Luna-Bárcenas JG, Mendoza-Galván A (2018) FTIR spectroscopy studies on the spontaneous neutralization of chitosan acetate films by moisture conditioning. Vib Spectrosc 94:1–6. https://doi.org/10.1016/j.vibspec.2017.10.005

Mohanasrinivasan V, Mishra M, Paliwal JS, et al (2014) Studies on heavy metal removal efficiency and antibacterial activity of chitosan prepared from shrimp shell waste. 3 Biotech, 4:167–175. https://doi.org/10.1007/s13205-013-0140-6

Nečas D, Klapetek P (2012) Gwyddion: An open-source software for SPM data analysis. Cent Eur J Phys 10:181–188. https://doi.org/10.2478/s11534-011-0096-2

Niamsa N, Baimark Y (2009) Preparation and characterization of highly flexible chitosan films for use as food packaging. Am J Food Technol 4:162–169. https://doi.org/10.3923/ajft.2009.162.169

No HK, Meyers SP (2000) Application of chitosan for treatment of wastewaters. Rev Environ Contam Toxicol 163:1–27

Noriega SE, Subramanian A (2011) Consequences of neutralization on the proliferation and cytoskeletal organization of chondrocytes on chitosan-based matrices. Int J Carbohydr Chem 2011:1–13. https://doi.org/10.1155/2011/809743

Ogawa K, Yui T, Okuyama K (2004) Three D structures of chitosan. Int J Biol Macromol 34:1–8

Rashid S, Shen C, Chen X et al (2015) Enhanced catalytic ability of chitosan–Cu–Fe bimetal complex for the removal of dyes in aqueous solution. RSC Adv 5:90731–90741. https://doi.org/10.1039/C5RA14711E

Reddy Tiyyagura H, Rudolf R, Gorgieva S et al (2016) The chitosan coating and processing effect on the physiological corrosion behaviour of porous magnesium monoliths. Prog Org Coatings 99:147–156. https://doi.org/10.1016/j.porgcoat.2016.05.019

Shariatinia Z (2019) Pharmaceutical applications of chitosan. Adv Colloid Interface Sci 263:131–194

Shen C, Chen H, Wu S et al (2013) Highly efficient detoxification of Cr(VI) by chitosan-Fe(III) complex: Process and mechanism studies. J Hazard Mater 244–245:689–697. https://doi.org/10.1016/j.jhazmat.2012.10.061

Takara EA, Marchese J, Ochoa NA (2015) NaOH treatment of chitosan films: impact on macromolecular structure and film properties. Carbohydr Polym 132:25–30. https://doi.org/10.1016/j.carbpol.2015.05.077

Wang X, Xi Z, Liu Z et al (2011) The fabrication and property of hydrophilic and hydrophobic double functional bionic chitosan film. J Nanosci Nanotechnol 11:9737–9740. https://doi.org/10.1166/jnn.2011.5327

Wang J, Gardner DJ, Stark NM et al (2018) Moisture and oxygen barrier properties of cellulose nanomaterial-based films. ACS Sustain Chem Eng 6:49–70

Wang W, Meng Q, Li Q, et al (2020) Chitosan derivatives and their application in biomedicine. Int J Mol Sci 21

Wetteland CL, de Jesus SJ, Silken CA et al (2018) Dissociation of magnesium oxide and magnesium hydroxide nanoparticles in physiologically relevant fluids. J Nanoparticle Res 20:1–17. https://doi.org/10.1007/s11051-018-4314-3

Yap WF, Yunus WMM, Talib ZA, Yusof NA (2011) X-ray photoelectron spectroscopy and atomic force microscopy studies on crosslinked chitosan thin film. Int J Phys Sci 6:2744–2749. https://doi.org/10.5897/IJPS11.121